Arch. Metall. Mater. **65** (2020), 4, 1317-1322

DOI: 10.24425/amm.2020.133692

HOCHEOL SONG[1], SEONGI LEE[1], KWANGMIN LEE[1*]

MICROSTRUCTURE AND ELECTROCHEMICAL BEHAVIORS OF EQUIATOMIC TiMoVCrZr AND Ti-RICH TiMoVCrZr HIGH-ENTROPY ALLOYS FOR METALLIC BIOMATERIALS

The present study investigated various thermodynamic parameters, microstructures and electrochemical behaviors of TiMoVCrZr and Ti-rich TiMoVCrZr high-entropy alloys (HEAs) prepared by vacuum arc remelting. The microstructures of the alloys were analyzed using X-ray diffraction (XRD) analysis, field emission scanning electron microscopy (FE-SEM), and potentiodynamic polarization tests. The determined thermodynamic values of the Ω-parameter and the atomic size difference (δ) for the HEAs were determined to be in the range of $\Omega \geq 1.1$, and $\delta \leq 6.6\%$ with valance electron configuration (VEC) ≤ 5.0, suggesting the HEAs were effective at forming solid solutions. XRD patterns of the equiatomic $Ti_{20}Mo_{20}V_{20}Cr_{20}Zr_{20}$ HEA revealed four phases consisting of the body centered cubic$_1$ (BCC_1), BCC_2, hexagonal close-packed (HCP), and intermetallic compound Cr_2Zr phases. Three phases were observed in the XRD patterns of Ti-rich $Ti_{40}Mo_{15}V_{15}Cr_{15}Zr_{15}$ (BCC, HCP, and Cr_2Zr) and a single BCC phase was observed in Ti-rich $Ti_{60}Mo_{10}V_{10}Cr_{10}Zr_{10}$ HEAs. The backscattered-electron (BSE) images on the equiatomic $Ti_{20}Mo_{20}V_{20}Cr_{20}Zr_{20}$ HEA revealed BCC and HCP phases with Cr_2Zr precipitates, suggesting precipitation from the HCP solid solution during the cooling. The micro-segregation of Ti-rich $Ti_{60}Mo_{10}V_{10}Cr_{10}Zr_{10}$ HEAs appeared to decrease remarkably. The alloying elements in the HEAs were locally present and no phase changes occurred even after additional HIP treatment. The lowest current density obtained in the polarization potential test of Ti-rich $Ti_{40}Mo_{15}V_{15}Cr_{15}Zr_{15}$ HEA was 7.12×10^{-4} mA/cm^2 was obtained. The studied TiMoVCrZr HEAs showed improved corrosion characteristics as compared to currently available joint replacement material such as ASTM F75 alloy.

Keywords: High Entropy Alloy, TiMoVCrZr, Hot Isostatic Pressing, Potentiodynamic polarization

1. Introduction

HEAs, alloys with five or more principal elements, with equiatomic or near equiatomic compositions provide unique properties in comparison to conventional alloys because of their high configurational entropy [1,2]. HEAs may favor the formation of single-phase solid solutions, such as face-centered cubic (FCC), BCC, or HCP; in other cases, they form two or more phases in other cases. Yeh et al proposed that the four core HEA effects, including high-entropy, sluggish diffusion, severe lattice distortion, and cocktail effects, all play a major role in improving physical and mechanical properties [3].

Most refractory HEAs based on the metallic elements of Group IV (Ti, Zr, and Hf), Group V (V, Nb, and Ta), and Group VI (Cr, Mo, and W) have exhibited a single BCC phase with high hardness and strength but insufficient ductility at room temperatures. Willmann suggested that the ideal materials for joint replacement should exhibit a biocompatibility, high hardness and stiffness, and an excellent corrosion resistance [4]. Co-28wt.%Cr-6wt.%Mo alloys (ASTM F75 in the cast version and ASTM F799 is the wrought version) are more wear-resistant, and are clinically used as femoral head surfaces of the joint prostheses. HEAs, being capable of the formation of single- or two-phase solid solutions, have the potential to improve performance of the joint prostheses. In addition, Ti-rich HEAs have the potential to prevent adverse fibrous tissue encapsulation reactions. A few studies on the electrochemical behaviors of TiZrTaHfNb [5], TiZrNbTaMo [6], and $TiZr_{0.5}NbCr_{0.5}V_xMo_y$ [7] HEAs showed remarkably high polarization resistance and superior pitting resistance when compared to CoCrMo alloys and 316L stainless steel.

The purpose of this study was to investigate various thermodynamic parameters, microstructures, and electrochemical behaviors of equiatomic and Ti-rich TiMoVCrZr HEAs as prepared by vacuum arc remelting.

[1] CHONNAM NATIONAL UNIVERSITY,SCHOOL OF MATERIALS SCIENCE & ENGINEERING, GWANGJU 61186, REPUBLIC OF KOREA

* Corresponding author: kmlee@jnu.ac.kr

2. Experimental

The $Ti_{20}Mo_{20}V_{20}Cr_{20}Zr_{20}$ HEA and the Ti-rich $Ti_{40}Mo_{15}V_{15}Cr_{15}Zr_{15}$ and $Ti_{60}Mo_{10}V_{10}Cr_{10}Zr_{10}$ HEAs were fabricated by vacuum arc remelting (VAR, ACE VACUUM, AVA-1500, Korea). Commercially pure Ti chips (ASTM CP Grade II), Mo bars (99.8 wt.%), V sheets (99.9 wt.%), Cr chips (99.9 wt.%) and Zr sheets (99.9 wt.%) were arc melted in a water-cooled copper hearth with a tungsten electrode. The ingots were subsequently flipped and re-melted five times in an argon atmosphere. All the cast ingots were then homogenized at 1000 and 1200°C for 4 h in a vacuum atmosphere with a pressure of 1.5×10^{-3} Pa. The actual chemical compositions (at%) of TiMoVCrZr HEAs analyzed using EDS attached FE-SEM are given in Table 1. Special heat treatment was applied with hot isostatic pressing (HIP, AIP10-30H, American Isostatic Presses, U.S.A.) at a temperature of 1300°C for 4 h with a pressure of 150 MPa.

TABLE 1

Actual chemical compositions (at%) of TiMoVCrZr HEAs analyzed using EDS attached FE-SEM

Alloy	Ti	Mo	V	Cr	Zr	Total
$Ti_{20}Mo_{20}V_{20}Cr_{20}Zr_{20}$	16.73	23.90	20.37	16.96	22.03	100.00
$Ti_{40}Mo_{15}V_{15}Cr_{15}Zr_{15}$	41.05	16.21	14.88	13.62	14.24	100.00
$Ti_{60}Mo_{10}V_{10}Cr_{10}Zr_{10}$	58.89	10.61	9.27	10.05	11.18	100.00

The phase constitutions of the HEAs were examined by X-ray diffraction (XRD, PANalytical, X' Pert pro, Netherland) analysis using Cu-Kα radiation over a 2θ range of 20-90° at an acceleration voltage of 40 kV. Field emission scanning electron microscopy (FE-SEM, Gemini 500, ZEISS, Germany) in conjunction with energy dispersive X-ray spectroscopy (EDS) were used to characterize the microstructures of the HEAs.

Electrochemical experiments were performed on a flat cell corrosion tester (PARSTAT 2273, USA) at a temperature of 37±1°C. A three-electrode cell was used for potentiodynamic polarization tests, where the reference electrode was a silver/silver chloride electrode, the counter electrode was made of a platinum plate, and the working electrode was the specimen. All experiments were conducted at a constant scan rate of 0.25 mV/s, initiated at −250 mV below the open-circuit potential. The working electrolyte was an aqueous Ringer's physiological solution (NaCl = 9.00 g L^{-1}; $CaCl_2$ = 0.24 g L^{-1}; KCl = 0.43 g L^{-1}; $NaHCO_3$ = 0.2 g L^{-1}).

3. Results and discussion

Thermodynamic parameters, including the enthalpy of mixing (ΔH_{mix}), the entropy of mixing (ΔS_{mix}), and the **Ω**-parameter [8], the (δ) [9], and the VEC [10], were used to predict the formation of solid solution of HEAs. Equations for these terms were expressed as:

$$\Delta H_{mix} = \sum_{i=1, i\neq j} \Omega_{ij} c_i c_j \tag{1}$$

$$\Delta S_{mix} = -R\sum_{i=1}^{n}(c_i \ln c_i) \tag{2}$$

$$\Omega = \frac{T_m \Delta S_{mix}}{\left|\Delta H_{mix}\right|} \tag{3}$$

$$\delta = 100\sqrt{\sum_{i=1}^{n} c_i \left(1 - \frac{r_i}{\bar{r}}\right)^2} \tag{4}$$

$$VEC = \sum_{i=1}^{n} c_i \left(VEC\right)_i \tag{5}$$

where $\Omega_{ij} = 4\Delta H_{mix}^{AB}$ was the regular solution interaction parameter between the i^{th} and j^{th} elements, c_i or c_j were the atomic percentage of the i^{th} or j^{th} components, ΔH_{mix}^{AB} was the enthalpy of mixing of binary alloys, R (8.314 J/K·mol) was the gas constant, $(T_m)_i$ was the melting point of the i^{th} component of alloy, $\bar{r} = \sum_{i=1}^{n} c_i r_i$ was the average atomic radius, r_i was the atomic radius, and VEC_i was the VEC for the i^{th} element.

Table 2 shows various thermodynamic parameters calculated using Eqs. (1), (2), (3), (4), and (5) for predicting the formation of solid solution phases in the TiMoVCrZr HEAs. The values of δ, **Ω**-parameter, and VEC were 6.8%, 5.73, and 5, respectively, for $Ti_{20}Mo_{20}V_{20}Cr_{20}Zr_{20}$; 5.9%, 6.32, and 4.75, respectively, for $Ti_{40}Mo_{15}V_{15}Cr_{15}Zr_{15}$; 4.3%, 7.39, and 4.5, respectively, for $Ti_{60}Mo_{10}V_{10}Cr_{10}Zr_{10}$. The obtained values of the **Ω**-parameter and the δ, were found in the range of $\Omega \geq 1.1$, and $\delta \leq 6.6\%$ [8], suggesting an effective formation of solid solutions. A slightly high value of δ (6.8%) was obtained for $Ti_{20}Mo_{20}V_{20}Cr_{20}Zr_{20}$ HEA. Additionally, all VEC values were less than 6.87 [10], indicating HEAs with BCC solid solutions.

TABLE 2

Thermodynamic parameters (δ, ΔH_{mix}, ΔS_{mix}, **Ω**, and VEC) used for predicting the formation of solid solution phases of TiMoVCrZr HEAs

Alloy	δ (%)	ΔH_{mix} (kJ/mol)	ΔS_{mix} (J/K·mol)	**Ω**	VEC
$Ti_{20}Mo_{20}V_{20}Cr_{20}Zr_{20}$	6.8	– 5.28	13.327	5.73	5.00
$Ti_{40}Mo_{15}V_{15}Cr_{15}Zr_{15}$	5.9	– 4.32	12.51	6.32	4.75
$Ti_{60}Mo_{10}V_{10}Cr_{10}Zr_{10}$	4.3	– 3.12	10.97	7.39	4.50

Fig. 1 shows XRD pattern of $Ti_{20}Mo_{20}V_{20}Cr_{20}Zr_{20}$, which was as-cast and heat-treated at 1000 and 1200°C for 4 h, and XRD patterns of $Ti_{40}Mo_{15}V_{15}Cr_{15}Zr_{15}$, and $Ti_{60}Mo_{10}V_{10}Cr_{10}Zr_{10}$, which were as-cast and heat-treated at 1300°C for 4 h and additional HIP treated at a temperature of 1300°C for 4 h with a pressure of 150 MPa after heat treatment at 1200°C for 4 h, respectively. Fig. 1(a) shows that four main X-ray peaks on the planes, (110), (200), (211), and (220), correspond to the BCC_1 phase. The BCC_2 solid solution phase with a peak at around 59 degrees in as-cast $Ti_{20}Mo_{20}V_{20}Cr_{20}Zr_{20}$ HEA divided into more stable BCC_1 and BCC_2 phases because of sufficient heat treatment effects at high temperatures. An occurrence in the phase

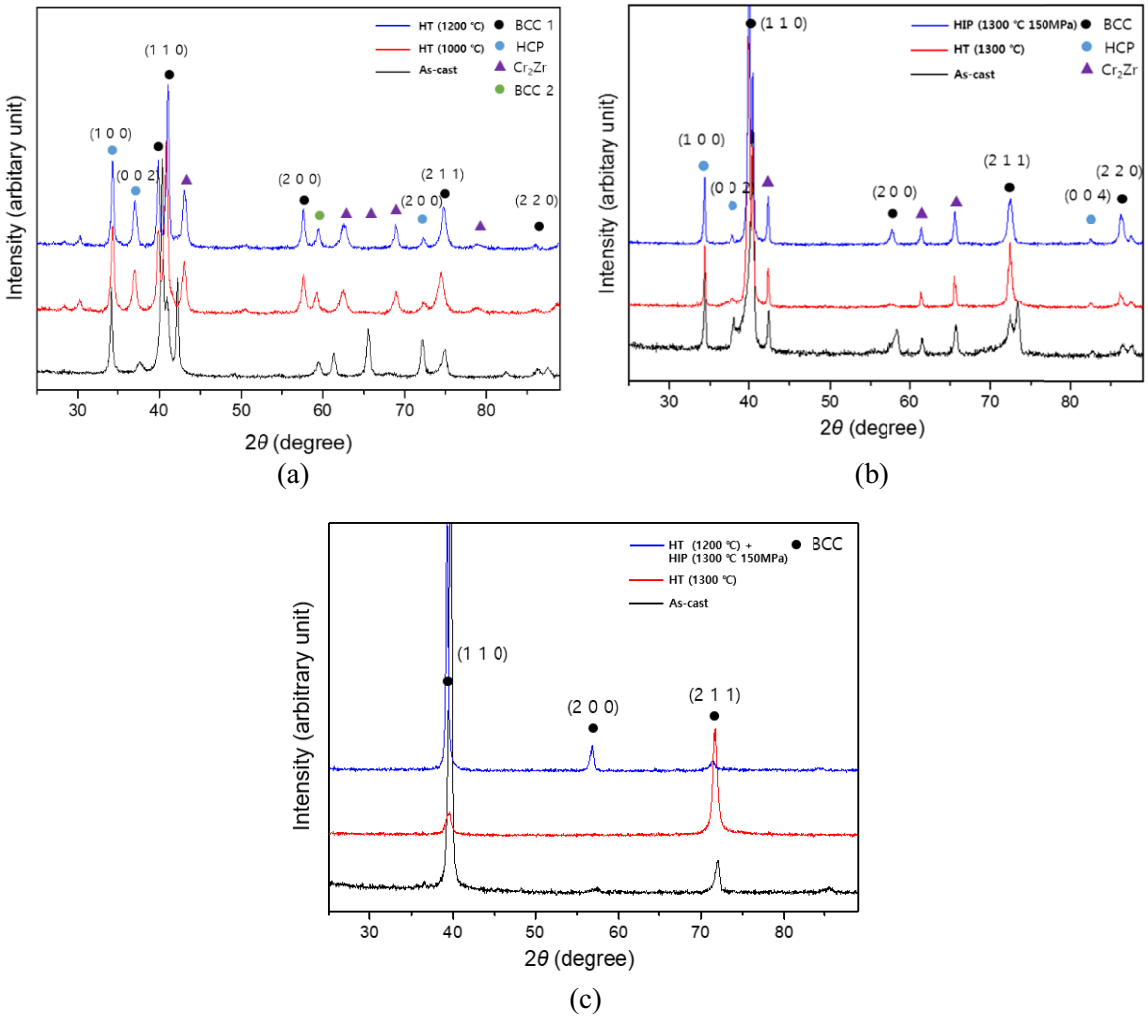

Fig. 1. XRD patterns of (a) the equiatomic $Ti_{20}Mo_{20}V_{20}Cr_{20}Zr_{20}$ HEA and (b) the Ti-rich $Ti_{40}Mo_{15}V_{15}Cr_{15}Zr_{15}$ and (c) $Ti_{60}Mo_{10}V_{10}Cr_{10}Zr_{10}$ HEAs

separation of the equiatomic $Ti_{20}Mo_{20}V_{20}Cr_{20}Zr_{20}$ can be attributed to the sluggish diffusion, regarded as one of the core effects of HEAs. In contrast, no BCC_2 phase for the HEAs with low alloying elements is observed in Figs. 1(b) and (c). X-ray peaks on the planes, (100), (002), and (200), are identified with the HCP phase. As shown in Fig 1(c), $Ti_{60}Mo_{10}V_{10}Cr_{10}Zr_{10}$ preserved its original BCC phase even after additional HIP processing. The Laves phase formation was expected when the atomic size ratio of the largest and smallest elements in the composition exceeds 1.225 [11]. The atomic size ratio of R_{Zr}/R_{Cr} was 1.242, wherease that of R_{Ti}/R_{Cr} was 1.131. Thus, the formation of the Cr_2Zr phase was expected in $Ti_{20}Mo_{20}V_{20}Cr_{20}Zr_{20}$ HEA. Li et al. [7] also suggested that the most negative enthalpy of mixing (–12 kJ/mol) between Cr and Zr may be favorable to form an intermetallic compound Cr_2Zr phase.

Fig. 2 shows the BSE SEM images and a series of EDS mapping of the alloying elements Ti, Mo, V, Cr, and Zr for the equiatomic $Ti_{20}Mo_{20}V_{20}Cr_{20}Zr_{20}$ and the Ti-rich $Ti_{40}Mo_{15}V_{15}Cr_{15}Zr_{15}$ and $Ti_{60}Mo_{10}V_{10}Cr_{10}Zr_{10}$ HEAs. As shown in the BSE images of Figs. 2(a) and (b), two mixed microstructures were observed because of the α-(HCP) or β-Ti (BCC) phase stabilizing elements. The alloying elements Mo and V associated with the formation of the BCC solid solutions were enriched together with Ti. The alloying elements Cr and Zr associated with the formation of the HCP solid solution were found in the same regions. The Laves phase of the Cr_2Zr phase could be precipitated from the HCP solid solution during the cooling. Some precipitates (white spots) can be seen in the BSE image of Fig. 2(a). In contrast, Fig. 2(c) reveals that micro-segregation of $Ti_{60}Mo_{10}V_{10}Cr_{10}Zr_{10}$ appeared to decrease remarkably.

Fig. 3 shows the BSE SEM image and EDS mapping of the alloying elements Ti, Mo, V, Cr, and Zr for the Ti-rich $Ti_{40}Mo_{15}V_{15}Cr_{15}Zr_{15}$ after the HIP treatment at a temperature of 1300°C with a pressure of 150 MPa. Additional HIP treatment after heat-treatment at 1200°C was applied to remove the constitutional micro-segregation of HEAs. However, as shown in Fig. 2(b), the two different microstructures (BCC + HCP) in HEAs were not significantly changed; the alloying elements remained locally even after additional HIP processing.

Fig. 4 shows the potentiodynamic polarization curves of the equiatomic $Ti_{20}Mo_{20}V_{20}Cr_{20}Zr_{20}$, the Ti-rich $Ti_{40}Mo_{15}V_{15}Cr_{15}Zr_{15}$ and $Ti_{60}Mo_{10}V_{10}Cr_{10}Zr_{10}$ HEAs. Corrosion behaviors relating to biocompatibility are the main factors involved in biomedical application. In general, E_{corr} and i_{corr} represent the

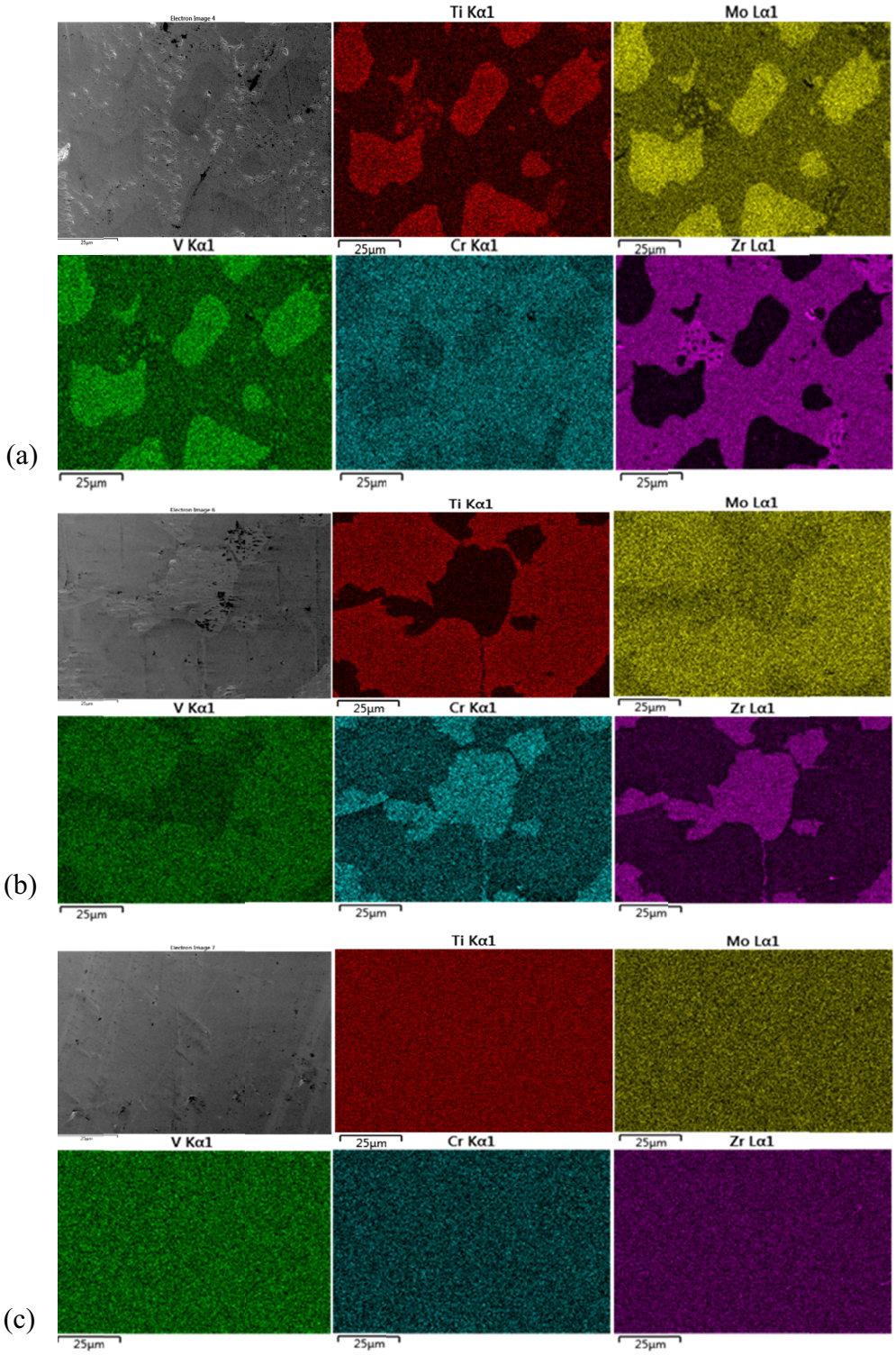

Fig. 2. BSE SEM images and EDS mapping of the alloying elements Ti, Mo, V, Cr, and Zr for TiMoVCrZr HEAs: (a) $Ti_{20}Mo_{20}V_{20}Cr_{20}Zr_{20}$, (b) $Ti_{40}Mo_{15}V_{15}Cr_{15}Zr_{15}$, and (c) $Ti_{60}Mo_{10}V_{10}Cr_{10}Zr_{10}$

corrosion potential and corrosion current density, respectively. As shown in the polarization graph in Fig. 4(a), no sign of oxygen evolution also was not observed in the cathodic branch. The passivation of the $Ti_{20}Mo_{20}V_{20}Cr_{20}Zr_{20}$ HEA occurred at a much higher current density than 10 uA and the breakdown potential was rather low at 1.2 V above the corrosion potential. In addition, it is worth noting that the slight increase in current density before the passivated film breakdown showed that the passivated film was not sufficiently strong. In contrast, Fig. 4(b) revealed a continuous passive plateau up to 1100 $mV_{Ag/AgCl}$ without breakdown potential, suggesting the high polarization resistance on the surface of the Ti-rich $Ti_{40}Mo_{15}V_{15}Cr_{15}Zr_{15}$ HEA without localized pitting corrosion because of a high electronegative element of Ti. A slight increase from the passive current without a rapid increase in the current density could maintain the consistency of the passivated layer. Fig. 4(c)

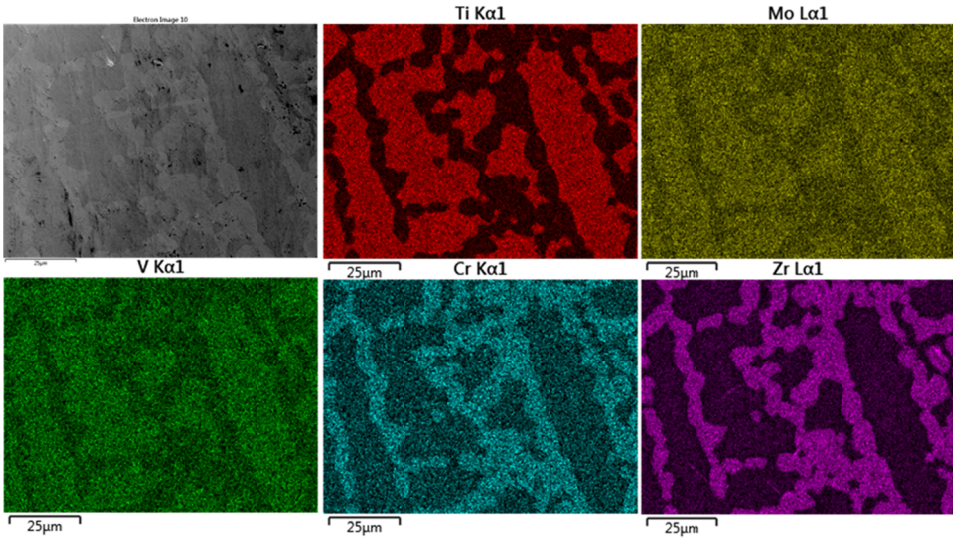

Fig. 3. BSE SEM images and EDS mapping of the alloying elements Ti, Mo, V, Cr, and Zr for $Ti_{40}Mo_{15}V_{15}Cr_{15}Zr_{15}$ HEA after HIP treatment at a temperature of 1300°C with a pressure of 150 MPa

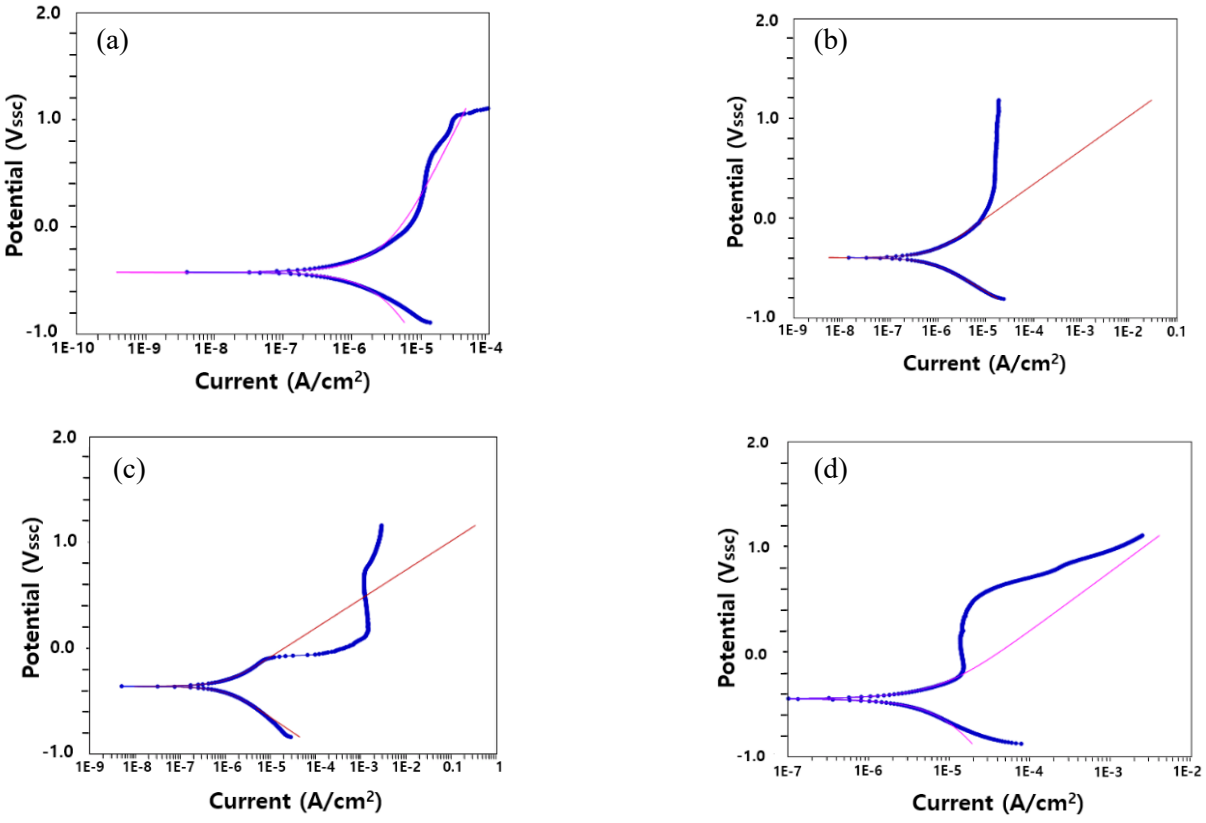

Fig. 4. Potentiodynamic polarization curves of (a) $Ti_{20}Mo_{20}V_{20}Cr_{20}Zr_{20}$, (b) $Ti_{40}Mo_{15}V_{15}Cr_{15}Zr_{15}$, (c) $Ti_{60}Mo_{10}V_{10}Cr_{10}Zr_{10}$ HEAs, and (d) ASTM F75 alloy

showed the passivated layer formed at a rather high current density (more than 1 mA) that was still comparable with $Ti_{40}Mo_{15}V_{15}Cr_{15}Zr_{15}$ HEA, even without any sign of breakdown at high potential.

The values of E_{corr} and i_{corr} obtained at potentiodynamic polarization curves of Fig. 4 are listed in Table 3. The lowest corrosion current density (7.12×10^{-4} mA/cm^2) was observed in the Ti-rich $Ti_{40}Mo_{15}V_{15}Cr_{15}Zr_{15}$ HEA, whereas the $Ti_{20}Mo_{20}V_{20}Cr_{20}Zr_{20}$ HEA showed the highest corrosion current density of 3.08×10^{-3} mA/cm^2. The values of E_{corr} for the HEAs increased from – 422 to – 356 mV with an increased amount of Ti; the Ti-rich HEAs showed better corrosion resistance than the equiatomic HEA. The present values of E_{corr} and i_{corr} were comparable with the other HEAs obtained in phosphate buffer solution electrolyte; E_{corr} and i_{corr} for TiZrTaHfNb [5] corresponded to – 391 mV and 0.072 μA/cm^2, similarly the values for TiZrTaMo [6]

were – 607 mV and 0.89 μA/cm^2, respectively. In comparison with currently available joint replacement material of ASTM F75 alloy, the corrosion resistance of $Ti_{20}Mo_{20}V_{20}Cr_{20}Zr_{20}$, $Ti_{40}Mo_{15}V_{15}Cr_{15}Zr_{15}$ and $Ti_{60}Mo_{10}V_{10}Cr_{10}Zr_{10}$ HEAs appeared superior.

TABLE 3

E_{corr} and i_{corr} values obtained at potentiodynamic polarization curves of Fig. 4

HEAs	**$Ti_{20}Mo_{20}V_{20}Cr_{20}Zr_{20}$**	**$Ti_{40}Mo_{15}V_{15}Cr_{15}Zr_{15}$**	**$Ti_{60}Mo_{10}V_{10}Cr_{10}Zr_{10}$**
E_{corr} (mV)	– 422	– 393	– 356
I_{corr} (mA/cm^2)	3.08×10^{-3}	7.12×10^{-4}	1.02×10^{-3}
Control	ASTM F75 (Co-28Cr-6Mo) (wt.%)		
E_{corr} (mV)	– 447		
I_{corr} (mA/cm^2)	7.34×10^{-3}		

4. Conclusion

In this study, various thermodynamic parameters, microstructures and electrochemical behaviors of the equiatomic TiMoVCrZr and Ti-rich TiMoVCrZr HEAs were investigated. The following results were derived from this study.

1. The thermodynamic values of the **Ω**-parameter and the δ for the HEAs were determined to be in the range of $\mathbf{\Omega} \geq 1.1$, and $\delta \leq 6.6\%$ with VEC ≤ 5.0, suggesting the HEAs were effective at forming solid solutions.
2. XRD patterns of the equiatomic $Ti_{20}Mo_{20}V_{20}Cr_{20}Zr_{20}$ HEA revealed four phases consisting of BCC_1, BCC_2, HCP, and intermetallic compound Cr_2Zr phase. An occurrence in the phase separation of the HEA could be explained by the sluggish diffusion of HEA. Three phases were observed in the XRD patterns of Ti-rich $Ti_{40}Mo_{15}V_{15}Cr_{15}Zr_{15}$ (BCC, HCP, and Cr_2Zr) and a single BCC phase was observed in Ti-rich $Ti_{60}Mo_{10}V_{10}Cr_{10}Zr_{10}$, preserving its original BCC phase even after HIP treatment at 1300 °C with a pressure of 150 MPa.
3. The BSE images on the equiatomic $Ti_{20}Mo_{20}V_{20}Cr_{20}Zr_{20}$ HEA revealed BCC and HCP phases with Cr_2Zr precipitates, suggesting precipitation from the HCP solid solution during the cooling. The micro-segregation of $Ti_{60}Mo_{10}V_{10}Cr_{10}Zr_{10}$ appeared to decrease remarkably.
4. The alloying elements in the HEAs were locally present and no phase changes occurred even after the additional HIP treatment.

The lowest corrosion current density obtained in the polarization potential test of Ti-rich $Ti_{40}Mo_{15}V_{15}Cr_{15}Zr_{15}$ HEA was 7.12×10^{-4} mA/cm^2. The Ti-rich HEAs showed better corrosion resistance than the equiatomic HEA. The studied TiMoVCrZr HEAs showed improved corrosion characteristics in comparison to currently available joint replacement material of ASTM F75 alloy.

Acknowledgments

This research was supported by the Basic Science Research Program of the National Research Foundation of Korea (NRF) funded by the Ministry of Education (NRF-2018R1D1A1B07041526).

REFERENCES

[1] B. Cantor, I.T.H. Chang, P. Knight, A.J.B. Vincent, Mater. Sci. Eng. **A 375-377**, 213 (2004).
[2] J.W. Yeh, S.K. Chen, S.J. Lin, J.Y. Gan, T.S. Chin, T.T. Shun, C.H. Tsau, S.Y. Chang, Adv. Eng. Mater. **6**, 299 (2004).
[3] J.W. Yeh, JOM. **65**, 1759 (2013).
[4] G. Willmann, Adv. Eng. Mater. **3**, 135 (2001).
[5] A. Motallebzadeh, N.S. Peighambardoust, S. Sheikh, H. Murakami, S. Guo, D. Canadinc, Intermetallics **113**, 106572 (2019).
[6] S.P. Wang, J. Xu, Mater. Sci. Eng. **C 73**, 80 (2017).
[7] J. Li, X. Yang, R. Zhu and Y. Zhang, Metals, **4**, 597 (2014)
[8] Y. Zhnag, Z.P. Lu, S.G. Ma, P.K. Liaw, Z. Tang, Y.Q. Cheng, M.C. Gao, MRS Commun. **4**, 57 (2014).
[9] Y. Zahng, Y.J. Zhou, J.P. Lin, G.L. Chen, P.K. Liaw, Adv. Eng. Mater. **10**, 534 (2008)**.**
[10] S. Guo, C. Ng, J. Lu, C.T. Liu, J. Appl. Phys. **109**, 103505 (2011).
[11] A.P. Hynninen, J.H.J. Thijssen, E.C.M. Vermolen, M. Dijkstra, A.V. Blaaderen, Nat. Mater. **6**, 202 (2007)